Journal of Solid State Chemistry 182 (2009) 2566–2578

Contents lists available at ScienceDirect

Journal of Solid State Chemistry

journal homepage: www.elsevier.com/locate/jssc

Effect of added zinc on the properties of cobalt-containing ceramic pigments prepared from layered double hydroxides

M.E. Pérez-Bernal, R.J. Ruano-Casero, V. Rives *

GIR-QUESCAT, Departamento de Química Inorgánica, Universidad de Salamanca, 37008 Salamanca, Spain

ARTICLE INFO

Article history:
Received 3 April 2009
Received in revised form
3 July 2009
Accepted 7 July 2009
Available online 30 July 2009

Keywords:
Layered double hydroxides
Hydrotalcite
Ceramic pigment
Spinel
X-ray diffraction
Colour parameters

ABSTRACT

Layered double hydroxides (LDHs) with the hydrotalcite-type structure containing Co and Al, or Zn, Co and Al in the brucite-like layers and carbonate in the interlayer have been prepared by coprecipitation. The Zn/Co molar ratio was kept to 1 in all samples, while the divalent/trivalent molar ratio was varied from 2/1 to 1/2. The samples have been characterised by element chemical analysis, powder X-ray diffraction, differential thermal and thermogravimetric analysis, temperature-programmed reduction and FT-IR spectroscopy. A single hydrotalcite-like phase is formed for samples with molar ratio 2/1, which crystallinity decreases as the Al content is increased, developing small amounts of diaspore and dawsonite and probably an additional amorphous phase. Calcination at 1200 °C in air led to formation of spinels; a small amount of $NaAlO_2$ was observed in the Al-rich samples, which was removed by washing. The nature of the spinels formed (containing Co^{II}, Co^{III}, Al^{III} and Zn^{II}) strongly depends on the cations molar ratio in the starting materials and the calcination treatment, leading to a partial oxidation of Co^{II} species to Co^{III} ones. Colour properties ($L^*a^*b^*$) of the original and calcined solids have been measured. While the original samples show a pink colour (lighter for the series containing Zn), the calcined Co,Al samples show a dark blue colour and the Zn,Co,Al ones a green colour. Changes due to the different molar ratios within a given calcined series are less evident than between samples with the same composition in different series. These calcined materials could be usable as ceramic pigments.

1. Introduction

Ceramic pigments are inorganic crystalline structures able to develop a stable colour at high temperatures. They should be thermally stable, resistant to alkaline and acid attacks, insoluble in glazes, to show a given narrow particle size distribution and should not evolve gases. Three different types are commonly described, namely, (i) those formed by an inorganic matrix including a chromophore in the structure or as a dopant in a solid solution, (ii) those formed by deposition of a colloidal layer of the chromophore on a support, and (iii) those where the chromophore is encapsulated in a crystalline carrier. The colour usually arises from charge transfer processes, electron transfer between energy bands, or *d–d* or *f–f* transitions. Llusar et al. [1] have reported a detailed analysis of cobalt-containing blue ceramic pigments with different crystalline phases, namely, olivine, willemite, and spinel; actually, the spinel structure is one of the most frequently found in ceramic pigments. The spinel structure is adopted by many compounds, but is extremely important for oxides with the stoichiometry $A^{II}B^{III}_2O_4$. The structure consists of a cubic close packing of oxide anions where the octahedral and tetrahedral holes are occupied by divalent or trivalent cations, giving rise to the so-called normal spinels (A^{II} in tetrahedral holes and B^{III} in octahedral ones) or inverse spinels (A^{II} and one half of B^{III} in octahedral holes and the remaining B^{III} cations in tetrahedral ones), together with partially inverse structures. The nature of the cations can be varied and, in addition, non-stoichiometric spinels (actually, mixtures where the spinels crystallites exist together with another oxide) are also known. If one or both cations correspond to transition metals, the solid shows a given colour, depending on the molar fraction of the metal cations, their formal oxidation state and the nature of holes occupied. Development of procedures to prepare spinels (both stoichiometric and non-stoichiometric) could be a good approach for obtaining ceramic pigments fulfilling the above listed requirements.

Although spinels can be prepared by a conventional ceramic reaction, alternative procedures have been described to obtain more homogeneous solids, with smaller particle size, under milder conditions. Regarding Co-containing spinels, hydrothermal methods [2,3] and sol–gel ones [4–7] have been applied. Meyer et al. [4] have used a microemulsion-assisted sol–gel process, using a single source heterometal alkoxide (containing both Al and the divalent cations) as a precursor; however, Lavrencic

* Corresponding author. Fax: +34 923 29 45 74.
E-mail address: vrives@usal.es (V. Rives).

0022-4596/$ - see front matter © 2009 Elsevier Inc. All rights reserved.
doi:10.1016/j.jssc.2009.07.011

Stangar et al. [6] have claimed that the use of two different cations precursors is much better, as it permits to vary the molar ratios between the cations, thus leading to formation of selected stoichiometric or non-stoichiometric spinels. The sol–gel and citrate procedures [5] permit formation of an intermediate homogeneous solid, favouring diffusion processes during thermal treatments, thus decreasing the temperature needed to form the desired compounds; similar advantages have been claimed [8] when using oxalate precursors. Pacurariu et al. [9] have used organometallic precursors (actually, Co^{II}, Zn^{II}, and Al^{III} nitrates reacted with 1,2-ethanediol) to prepare spinels with different Co/Zn molar ratios. Other methods, namely, auto-ignited gel combustion using citric acid as fuel and metal nitrate as oxidants [10], microemulsions [11], and the polymeric precursor [12] process, have been also applied. We report here on an alternative method, consisting of calcination of layered double hydroxides (LDHs). These are layered materials which structure corresponds to that of brucite, $Mg(OH)_2$, with partial Mg^{II}/M^{III} substitution. The positive charge of the layers is balanced by intercalated hydrated anions. The most representative member of this family of compounds is hydrotalcite, $Mg_6Al_2(CO_3)(OH)_{16}\cdot 4H_2O$. The cations can be easily changed (most of first transition metal cations, as well as Zn, Mg, Ga, In, etc., have been used to prepare different LDHs) and the divalent/trivalent molar ratio can be also changed within a rather broad range, as well as the interlayer anion (e.g., carbonate, chloride, nitrate, sulphate, polyoxometalates, anionic coordination compounds, etc.) [13–19]. We have previously reported on some of their applications in medicine as antacids and drug carriers [20], as anion scavengers [21,22], catalysts [23–26], catalyst supports and catalyst precursors [27–30].

We have also previously reported on the preparation of non-stoichiometric spinels containing Co and Fe [31], Ni, Co, Fe, and Al [32] and Ni and Fe [33] and we have studied their physicochemical properties and colour properties, specially analysing the changes arising from different molar ratios of the component cations. Studies have been also reported on the effect of doping by small amounts of a given cation for enhancing the colour [34], as well as the use of surfactants to obtain pigments with a narrow particle size distribution [35]. Systems containing other transition metal cations have been also studied [36–40]. One of the advantages of using LDHs as precursors for the pigment spinels is that we can modulate the properties of the calcined solids from the properties of the hydrotalcite-type precursors, and so such properties can be established beforehand. Preparation of Co-containing LDHs has been also described using microwaves as the heating medium, a method which permits a fine control of the particle size [41] and also avoids oxidation and formation of Co^{III} species [42]. The properties of LDHs and of the mixed oxides formed upon their calcinations when both Co and Cu exist in the interlayer, together with Al, strongly depend on the molar Cu/Co ratio [43].

In this paper, we present a comprehensive study of ceramic pigments prepared from LDH precursors containing cobalt and aluminum. It is well known that Co^{II} ions are responsible for the deep blue colour of ceramic pigments [1,44], because of their location in tetrahedral holes of the structure, where Laporte-partially allowed (by d–p mixing), spin-allowed transitions would occur, thus accounting for the intense colour observed. Such a location is observed in normal Co^{II}-containing spinels. On the other hand, it is also known that Zn^{II} cations behave as lattice modifiers, and consequently are able to tune very precisely the colour of the solid [45]. We have prepared two series of samples (without or with zinc), varying the divalent/trivalent molar ratio between 2/1 (stoichiometric LDH, leading to non-stoichiometric spinels) and 1/2 (non-stoichiometric LDH, leading to a stoichiometric spinel). The fact that Co^{II} species can undergo oxidation to the trivalent state and thus are able to substitute some of the Al^{III} cations from their positions, gives rise to interesting changes in the properties of these solids and consequently on their application as ceramic pigments. The samples prepared have been characterised using several physicochemical techniques and colour parameters ($L^*a^*b^*$) have been also determined.

2. Experimental

2.1. Sample preparation

All chemicals were from Panreac (PRS, puris.) and were used without any further purification. The samples were prepared by slow addition of a solution of the metal chlorides on a basic solution (NaOH and $NaHCO_3$), at room temperature. The total metal cations concentration was 2 M, the volume of the basic solution was twice that of the metal cations solution, and the HCO_3/Al molar ratio was fixed to unity. No insoluble residues were observed in the solutions before mixing.

Five samples with Co and Al were prepared, with nominal molar ratios (Co/Al) of 2/1, 3/2, 1/1, 2/3, and 1/2. For the five samples of the Zn, Co/Al system the same divalent/trivalent molar ratios were used, but with a Zn/Co molar ratio of 1/1 in all five cases.

Immediately after mixing the solutions, a pink precipitate was formed. Addition took 3–4 h, while the mixture was being mechanically stirred (400 ± 10 rpm, Heidolph mod. RZR-Z051 vertical stirrer). Stirring was continued during 14–20 h after addition was complete. The solids were then filtered in a Büchner funnel (20 cm diameter) with a water vacuum pump.

The mother liquids were colourless; this is not unexpected, as Al aquocomplexes are colourless and $[Co(H_2O)_6]^{2+}$ species display a weak pink colour. pH ranged between 9.3 and 9.9. Analysis showed the presence of a maximum of 0.16 ppm Co and 0.5 ppm Al for the Co/Al samples, but for the ternary samples the amount of Al was 1.11–2.19 ppm, while Zn was not detected and Co was between 0.19 and 0.30 ppm.

The dried solids were washed with four portions of 150 mL of distilled water each and a final portion of 500 mL. In each washing step the solid was maintained in contact with water for 30 min before connecting the water vacuum pump. Washing liquids were colourless and pH varied in the 9.3–10.1 range. Air was flowed through the cake for 2 h after the fifth washing step and the solid was then spread on a glass plate to dry at room temperature for 4–5 days, and then it was manually ground in an agate mortar.

Samples of the Co/Al system will be named as CoAl0*X*, where $X=1$, 2, 3, 4, and 5 stand for the nominal Co/Al molar ratios of 2/1, 3/2, 1/1, 2/3, and 1/2, respectively. For the Zn,Co/Al system, samples will be named ZnCoAl0*X*, with the same meaning for *X*.

In order to prepare the mixed oxides, the samples were calcined up to 1200 °C at a heating rate of 5 °C/min, with a retention time of 5 h; after that the samples were let to cool freely. These calcined samples will be named as CoAl0*X*/1200 (or ZnCoAl0*X*/1200).

2.2. Characterisation

Element chemical analysis for metals was carried out at Servicio General de Análisis Químico Aplicado (University of Salamanca) by atomic absorption after dissolving the samples in nitric acid, in a Mark-II ELL-240 instrument. Carbon was analysed in a model CHNS-932 LECO elemental analyzer.

The powder X-ray diffraction (PXRD) patterns were obtained in a Siemens D-500 diffractometer using Cu Kα radiation ($\lambda=1.5450$ Å) connected to a DACO-MP microprocessor using Diffract-AT software. The applied power was 1200 W (40 kV and 30 mA). The scan speed was 2° (2θ)/min, and the crystalline

phases were identified using Eva (Graphics Evaluation Program) software, the ASTM files (Joint Committee on Powder Diffraction Standards (JCPDS)) and literature data.

Differential thermal analyses (DTA) were recorded in a DTA-7 model instrument from Perkin-Elmer, and the thermogravimetric analyses (TG) in a TGA7-HT model thermobalance also from Perkin-Elmer, in oxygen flow (30 mL/min). Both instruments were connected to a personal computer through TAC 7/DX interfaces, and the data were analysed using standard software (Pyris, Series Thermal Analysis system, version 3.0) also provided by Perkin-Elmer. This software also allowed us to determine the derivative TG curves (DTG). The heating rate was 10 °C/min in both cases and the final temperature reached was 900 °C (TG) or 1200 °C (DTA).

Temperature-programmed reduction (TPR) studies were carried out in a TPR/TPD 2900 model instrument from Micromeritics, equipped with a W–Au thermal conductivity detector and connected to an Olivetti mod. 300-28 acquisition data station. The reducing agent was a 5% (vol) H_2/Ar mixture from L'Air Liquide, circulated through the sample at a flow of 60 mL/min; a heating rate of 10 °C/min and a sample mass of 50 mg were used in order to optimize the analysis. The amount of hydrogen consumed was determined upon integration of the areas under the peaks, after calibrating the instrument with CuO (from Merck).

The FT-IR spectra were recorded in a M-1700 2B model spectrometer from Perkin-Elmer, using Spectrum V.200 software, in the 4000–400 cm^{-1} range. The samples were prepared in KBr discs (ca. 1 mg sample/300 mg KBr). Fifty scans were recorded at a nominal resolution of 4 cm^{-1} to improve the signal-to-noise ratio.

The nitrogen adsorption–desorption isotherms of nitrogen at −196 °C were recorded in an automatic volumetric instrument from Micromeritics (Gemini). A portion of 100 mg of sample was used, which had been previously degassed in a Flow Prep instrument (also from Micromeritics) at 110 °C under a nitrogen flow for 2–3 h.

Particle size distribution curves were determined in a Mastersizer 2000 instrument, from Malvern, by laser diffraction. The laser beam is focused on a cell containing the sample suspended in water, and becomes dispersed at different angles depending on the size of the solid particle. The samples were dispersed in water using a Hydro 2000G accessory under ultrasounds for 5 min. The instrument is connected to a PC and the data are treated with commercial Mastersizer software.

Colour of the samples was quantified by using a Konica Minolta colorimeter (Chroma Meter CR 400 model), equipped with a pulsed Xenon lamp. The data were collected by a personal computer through a RS-232 interface, and were analysed with Colour Data CM-100 W Spectra Magic NX software. We used the $L^*a^*b^*$ system (also known as CIELAB) as the colour space, where L^* stands for lightness ($L^* = 0$ for black and $L^* = 100$ for white), and a^* and b^* are chromaticity coordinates, where negative values for a^* indicate green, while positive values indicate red, and negative values for b^* indicate blue and positive values indicate yellow. Three measurements (with three twinkles each) on three different spots were taken for each sample, averaging the results. Samples were placed between flat colourless glasses on a black sample holder. The instrument had been previously calibrated with Minolta white reference CR-A 43 (*XYZ* parameters 0.3133, 93.80, and 0.3194, respectively).

3. Results and discussion

3.1. Element chemical analysis

Data for CoAl0*X* samples are summarised in Table 1. The Co/Al molar ratios are acceptably coincident with the nominal ones and sodium was also found. Although the amount of sodium could be decreased by increasing the number of washing cycles, the concomitant decrease in pH of the washing liquids would give rise to protonation of interlayer carbonate species. The nominal Al/C ratio for a hydrotalcite-type structure should be equal to 2.0, but the experimental values were always lower and roughly decreased as the Al content was increased. This could be due to the presence of carbonate (or hydrogencarbonate) adsorbed on the external surface of the crystallites or to the presence of Al species forming an additional phase, besides the hydrotalcite-type one. An increase in aluminum gives rise also to an increase in the amount of retained sodium in the solid.

Table 1
Element chemical analysis data for the solids and the washing liquids, lattice parameters, crystallite size, specific surface area and temperature-programmed reduction results for samples CoAl0*X*.

Sample	CoAl01	CoAl02	CoAl03	CoAl04	CoAl05
Co[a]	36.71	33.83	24.62	18.76	14.93
Al[a]	7.78	9.05	10.41	11.66	12.34
Na[a]	–	0.63	3.25	4.47	4.61
C[a]	2.09	2.36	3.40	4.00	3.79
Co/Al molar ratio (nominal)	2.00	1.50	1.00	0.67	0.50
Co/Al molar ratio (experimental)	2.16	1.71	1.08	0.74	0.55
Al/C molar ratio	1.64	1.69	1.35	1.28	1.43
Co[b]	0.11	0.12	0.16	0.10	0.12
Al[b]	0.13	0.42	0.11	0.51	n.d.
pH of mother liquor	9.3	9.6	9.4	9.7	9.6
Lattice parameter *a* (Å)[c]	3.06	3.06	3.06	3.04	3.06
Lattice parameter *c* (Å)[c]	22.80	22.81	22.68	22.74	22.84
Crystallite size *D* (Å)	270	90	91	90	100
Number of layers	36	12	12	12	13
Specific surface area (m^2/g)	45	54	53	53	56
TPR – H_2 consumption (exptl./theor.)	1.04	1.04	1.10	1.31	1.31

[a] Weight percentage.
[b] In the mother liquour (ppm).
[c] For the hydrotalcite-type structure.

Data for the Zn,Co/Al samples are summarised in Table 2. The divalent/trivalent and Zn/Co molar ratios are acceptably coincident with the nominal values. The Na content is lower than in the corresponding samples of the Co/Al system and it is absent for samples ZnCoAl01 and ZnCoAl02. The Al/C ratios are also lower than the value (2.00) for a stoichiometric hydrotalcite structure.

3.2. Powder X-ray diffraction analysis

The X-ray powder diffraction patterns of all 10 samples are shown in Fig. 1. The diagrams have been vertically displaced and the same scale has been used in both plots for an easier comparison.

All of them show diffraction lines due to the hydrotalcite structure. As the nominal M^{II}/Al ration is decreased, the peaks become weaker and worse defined, as previously reported by other authors [46], while some other minor diffraction maxima develop. The overall lower intensity of the peaks as the relative Al content is increased can be related to a worse crystallinity of the samples.

The diagrams for samples CoAl01 and ZnCoAl01 coincide with that of (JCPDS file 38-0486) $Zn_6Al_2(CO_3)(OH)_{16}\cdot 4H_2O$, with the hydrotalcite-type structure, and only minor differences, probably due to the different nature of the cations in the brucite-like layers, can be found. The relative intensities of the maxima due to the hydrotalcite-type phase decrease on increasing the Al content, but the positions remain almost unchanged, and new maxima develop, some of which (see Fig. 1) can be attributed to the presence of diaspore, AlO(OH) (JCPDS file 05-0355). Other diffraction maxima can be tentatively ascribed to the presence

of dawsonite, $NaAl(CO_3)(OH)_2$ (JCPDS file 19-1175). The presence of an excess of aluminum favours retention of sodium in the solid and formation of these new phases. In addition, the presence of non-crystalline phases in these Al-rich samples (e.g., amorphous Al oxohydroxides) cannot be ruled out.

From the positions of the first two maxima (from low diffraction angles) due to the hydrotalcite phase and assuming a 3R packing for the brucite-like layers, due to planes (003) and (006), respectively, lattice parameter c has been calculated as [47–49]

$$c = 3[(1/2)(d_{003} + 2d_{006})]$$

Table 2
Element chemical analysis data for the solids and the washing liquids, lattice parameters, crystallite size, specific surface area and temperature-programmed reduction results for samples ZnCoAl0*X*.

Sample	ZnCoAl01	ZnCoAl02	ZnCoAl03	ZnCoAl04	ZnCoAl05
Zn[a]	16.88	15.46	11.02	8.29	7.21
Co[a]	17.45	14.26	10.49	7.88	6.69
Al[a]	6.73	8.10	9.23	9.52	11.09
Na[a]	–	–	2.78	3.11	4.70
C[a]	2.09	2.20	3.20	3.36	3.17
(Zn+Co)/Al molar ratio (nominal)	2.00	1.50	1.00	0.67	0.50
(Zn+Co)/Al molar ratio (experimental)	2.22	1.59	1.01	0.74	0.55
Zn/Co molar ratio (experimental)	0.87	0.96	0.96	0.95	0.97
Al/C molar ratio	1.43	1.63	1.28	1.26	1.55
Zn[b]	–	–	–	0.92	-
Co[b]	0.30	0.27	0.27	0.19	0.29
Al[b]	2.13	1.11	1.12	1.33	2.19
pH of mother liquor	9.5	9.8	9.7	9.7	9.4
Lattice parameter a (Å)[c]	3.06	3.06	3.06	3.06	3.06
Lattice parameter c (Å)[c]	22.78	22.75	22.78	22.62	22.83
Crystallite size D (Å)	100	80	70	70	70
Number of layers	13	11	10	9	9
Specific surface area (m^2/g)	51	57	46	45	40
TPR–H_2 consumption (exptl./theor.)	1.46	1.50	1.42	1.40	1.53

[a] Weight percentage.
[b] In the mother liquor (ppm).
[c] For the hydrotalcite-type structure.

The value for lattice parameter a has been calculated from the position of the first maximum of the doublet close to 60° (2θ) due to diffraction by planes (110):

$$a = 2d_{110}$$

From the values for the lattice parameters, indexing in Fig. 1 has been made following the method proposed by Gay [47].

The values calculated for both parameters for all 10 samples are summarised in Tables 1 and 2. They are within the range reported for many different solids with the hydrotalcite-type structure [50]. Only minor (less than 1%) variations in the value of c are observed; the average value is 22.71 Å for samples Co/Al is and 27.75 Å for samples Zn,Co/Al These values are in agreement with location of the carbonate anions in the interlayer with their molecular plane parallel to the brucite-like layers.

The values of lattice parameter a are essentially identical for all 10 samples, 3.06 Å, as expected from the similar ionic radii of Zn^{2+} and Co^{2+} in octahedral coordination (high-spin for cobalt) are 0.88 and 0.885 Å, respectively [51]. However, as the aluminum content is increased a decrease in the value of lattice parameter a would be expected, as its ionic radii is 0.675 Å [51]. The fact that the value of a remains constant suggests that the progressively increased amount of aluminum existing in the samples is not incorporated into the hydrotalcite-type structure, but is segregated forming an additional phase, as confirmed by the presence of, at least, dawsonite and diaspore in these Al-rich samples.

From the element chemical analysis data in Tables 1 and 2, and assuming that cobalt cations are all in the divalent state, that no extra-hydrotalcite phases containing Zn or Co exist, and that the excess of aluminum (above that corresponding to a divalent/Al molar ratio of 2) has been segregated to form oxohydroxides or oxides, the formulae shown in Table 3 have been calculated. These are not obviously the real ones (which determination is probably impossible with the experimental techniques available to us), as for an easier formulation we assume that Al is forming alumina and we are ignoring the presence of non-crystalline phases. The water content has been determined from the TG results (see below) and corresponds to water molecules existing in the interlayer of the hydrotalcite-type crystallites, and hydration of the Al-containing species. From the FT-IR spectroscopy results shown below we have also assumed that carbonate is the only anion existing in the interlayer.

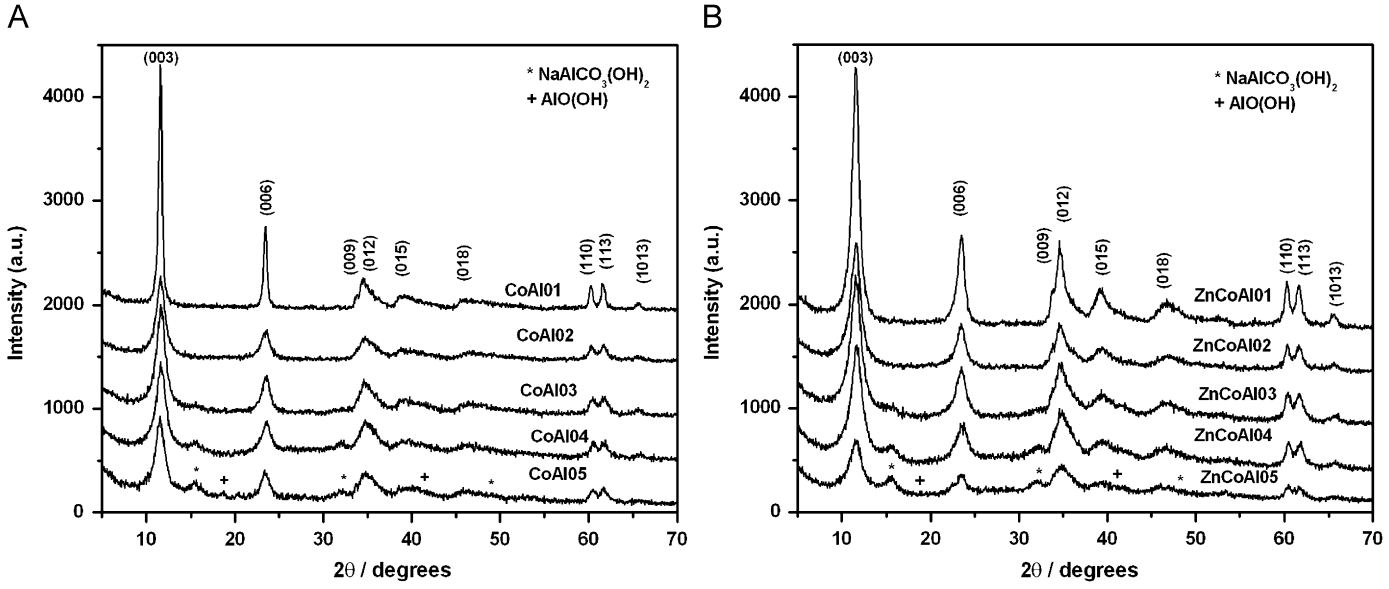

Fig. 1. Powder X-ray diffraction diagrams of samples (A) CoAl0*X*, and (B) ZnCoAl0*X*.

As the aluminum content increases above the $M^{II}/Al = 2$ ratio, the relative content of hydrotalcite decreases and a worse crystallinity seems to exist. The crystallite sizes, as calculated using the Scherrer formula from the width at half height of the diffraction maxima due to planes (003) and (006), for all 10 samples are also given in Tables 1 and 2. The instrumental broadening was determined using LaB_6 as internal reference [52,53] and the sizes calculated correspond to the height of the lamellar particles. The crystallite size decreases as the aluminum content increases for the Zn-containing samples, while for the Zn-free samples a sharp decrease is observed on passing from sample CoAl01 to the other samples within this series (270 to ca. 90–95 Å). For a given M^{II}/M^{III} ration, the presence of zinc gives rise to a decrease of the crystallite size. Taking an average value of 7.59 Å for the width of a layer–interlayer pair, the calculated number of layers in the average crystallites are also included in Tables 1 and 2.

The maximum amount of water molecules able to be packed in the interlayer space of the LDH can be calculated (per formula of hydrotalcite) as 2–3*x*, where *x* stands for the mole of carbonate per formula containing two hydroxyl groups (as written in Table 3). The values calculated for each sample are given in Table 3, and for samples CoAl01 and ZnCoAl01 are ca. one half of the amount of water measured from the TG curves. As the aluminum content increases, the amount of water exceeds the maximum calculated value, suggesting the formation, together with the hydrotalcite phase, of other highly hydrated and/or hydroxylated phase(s).

3.3. Thermal analyses

As the analyses were carried out in flowing oxygen, oxidation processes involving Co^{II} species are expected. The DTA curves are included in Fig. 2. No thermal effects are evident above ca. 500 °C and the TG curves show only an almost negligible mass loss above 500 °C (Fig. 3). The DTA curve for sample CoAl01 shows a single endothermic effect at 240 °C followed by an exothermic one at 295 °C, which suggests oxidation of Co^{II} species to Co^{III} ones. This behaviour is similar to those previously reported by other authors [54–56] for LDHs containing oxidizable cations in the brucite-like layers, the exothermic effect being absent when the analysis was carried out in an inert (nitrogen) atmosphere [56]. The endothermic effect for sample ZnCoAl01 is recorded at 210 °C without any exothermic effect, and a second, weaker, endothermic effect is recorded at 265 °C, suggesting that the oxidation of Co^{II} to Co^{III} is somewhat impeded in the presence of zinc. The shift of the minimum from 240 °C (sample CoAl01) to 210 °C (sample ZnCoAl01) should be related to the lower stability of $Zn(OH)_2$, which decomposes at 175 °C, shifting towards lower temperatures the overall decomposition of the LDH [57]. Both patterns show also a weak broad endothermic effect at lower temperatures, almost from room temperature, which can be attributed to removal of weakly (physically) adsorbed water; the strong effect is due to removal of water through condensation of layer hydroxyl groups and of carbon dioxide from interlayer carbonate species. This decomposition pattern has been confirmed for Mg,Al systems by mass spectrometry or temperature-programmed desorption [58,59]. The increase in the intensity of the first endothermic effect cannot be merely ascribed to removal of physically adsorbed water, as in such a case a direct correlation between the intensity of the effect and the amount of mass lost (as measured from the TG curves, see below) would be almost constant for the Zn-free samples (with an almost constant specific surface area, see Table 1), and would even decrease for the Zn-containing samples, as their specific surface area roughly decrease (Table 2) as the aluminum content is increased.

When the aluminum content increases the intensity of the low-temperature endothermic effect is progressively enhanced. The single endothermic effect for the Zn-free samples splits into two endothermic effects, which become weaker as the aluminum content is increased, and move apart each other, and the exothermic effect is almost undetected. For the Zn-containing samples two endothermic effects persist, but shift towards higher temperatures (10–15 °C) than for sample ZnCoAl01.

Development and strengthening of the low-temperature effect further confirms the presence of hydrated oxides or oxohydroxides of aluminum as its content increases.

The TG curves (Fig. 3), show a continuous mass loss; as the aluminum content increases more mass is lost at lower temperatures, in agreement with the enhancement in the intensity of the first endothermic peak at ca. 130 °C. The DTG curves (also included in Fig. 3) show a complex structure, with predominating peaks at 200–250 °C for the Al-poor samples, and the enhancement of a peak at ca. 100–125 °C for the Al-rich sample within each series. At the same time, a weak peak close to 300 °C develops for the Al-rich samples in both series.

Decomposition of these samples can be described in two steps, the first roughly extending from room temperature up to 550–600 °C, and the second one from this temperature to 1000 °C, where an almost flat TG curve is recorded. In the first step, water released at low temperature corresponds to hydration of the extra-hydrotalcite phases (probably aluminum oxohydroxides); then, condensation of the layer hydroxyl groups leads to further release of water, together with carbon dioxide from interlayer carbonate, leading to collapsing of the structure. The

Table 3
Proposed formulae for the solids prepared.

Sample	LDH		Al_2O_3	H_2O[a]	
	Formula in the anhydrous form	Fraction[a]	Fraction[a]	Exptl.	Calc.
CoAl01	$Co_{0.684}Al_{0.316}(OH)_2(CO_3)_{0.158}$	1	–	0.75	1.53
CoAl02	$Co_{0.667}Al_{0.333}(OH)_2(CO_3)_{0.166}$	0.97	0.03	1.04	1.47
CoAl03	$Co_{0.667}Al_{0.333}(OH)_2(CO_3)_{0.166}$	0.88	0.12	1.66	1.33
CoAl04	$Co_{0.667}Al_{0.333}(OH)_2(CO_3)_{0.166}$	0.78	0.22	2.10	1.19
CoAl05	$Co_{0.667}Al_{0.333}(OH)_2(CO_3)_{0.166}$	0.70	0.30	2.59	1.06
ZnCoAl01	$Zn_{0.321}Co_{0.369}Al_{0.310}(OH)_2(CO_3)_{0.155}$	1	–	0.75	1.52
ZnCoAl02	$Zn_{0.329}Co_{0.337}Al_{0.333}(OH)_2(CO_3)_{0.166}$	0.96	0.04	1.20	1.46
ZnCoAl03	$Zn_{0.324}Co_{0.342}Al_{0.333}(OH)_2(CO_3)_{0.166}$	0.86	0.14	1.95	1.31
ZnCoAl04	$Zn_{0.324}Co_{0.342}Al_{0.333}(OH)_2(CO_3)_{0.166}$	0.78	0.22	3.39	1.18
ZnCoAl05	$Zn_{0.328}Co_{0.338}Al_{0.333}(OH)_2(CO_3)_{0.166}$	0.69	0.31	3.90	1.05

[a] Mol per formula.

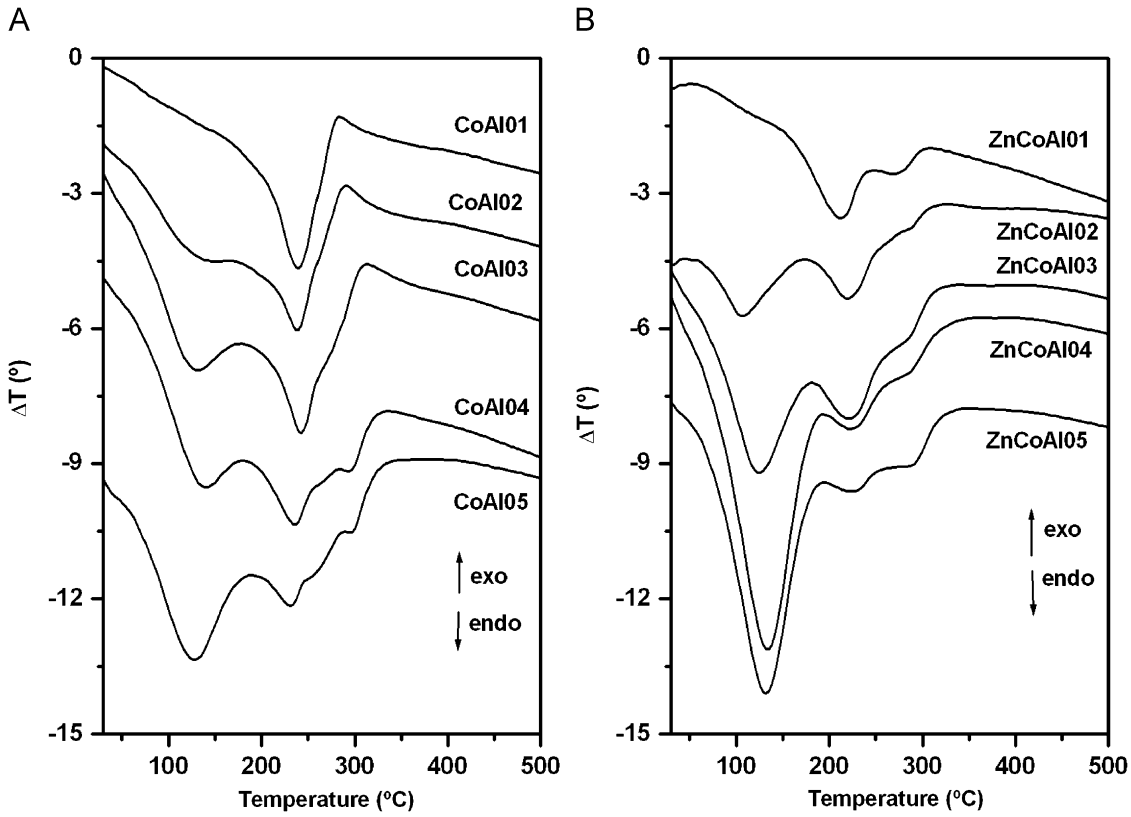

Fig. 2. Differential thermal analysis curves for samples (A) CoAl0*X*, and (B) ZnCoAl0*X*.

mass loss percentage in this first step increases with the aluminum content (as it includes dehydration of aluminum oxohydroxides), ranging from ca. 31% (sample CoAl01) to 44% for sample CoAl05.

The second step would extend from ca. 550 to 1000 °C. The mass loss is markedly lower (1–3% of the initial sample mass) and should correspond to removal of strongly held hydroxyl and/or carbonate anions, but reduction (to the divalent state) of cobalt species previously oxidized to the trivalent state at lower temperature cannot be discarded. Its value is ca. 2.7% for sample CoAl01 and decreases as the aluminum content is increased, i.e., as the molar fraction of LDH decreases (see the PXRD patterns). To insight in the decomposition process, we have recorded the PXRD patterns of the residues after the DTA study at 1000 °C.

The residue for sample CoAl01 shows only the diffraction lines of $Co^{II}Co^{III}AlO_4$ (Co_2AlO_4, JCPDS file 38-0814). From the Co and Al content in this sample (Table 1) the formula can be written as $Co_{2.05}Al_{0.95}O_4$, roughly close to the stoichiometric one Co_2AlO_4. The residues for the other Zn-free samples show the diffraction lines of this spinel, and peaks due to $NaAlO_2$ (JCPDS file 33-1200), which intensities increase with the Al (and Na) content.

The behaviour is rather similar for the Zn-containing samples. However, in this case, up to three different species with the spinel structure can be formed, namely, Co_2AlO_4 (JCPDS file 38-0814), $ZnAl_2O_4$ (gahnite, JCPDS file 05-0669) and $ZnCo_2O_4$ (JCPDS file 01-1149). Due to the similar ionic radii of Zn^{II} and Co^{II} cations both in tetrahedral (0.74 and 0.72 Å, respectively) and high-spin, octahedral (0.88 and 0.885 Å, respectively) [51] sites, no definite conclusion can be reached about the precise nature of the spinel formed; moreover, all Co_3O_4, $CoAl_2O_4$, $ZnAl_2O_4$, and $ZnCo_2O_4$ spinels adopt the normal structure. As for the other series of samples, the presence of sodium in the Al-rich samples gives rise to formation of $NaAlO_2$.

3.4. FT-IR spectroscopy

The spectra for selected samples from each series are included in Fig. 4; the spectra have been vertically displaced. No relevant differences are found for the set of samples with the same divalent/Al molar ratio.

The spectra are dominated by a broad, very intense band extending from ca. 3700 to 3000 cm^{-1}, due to the stretching mode of hydroxyl groups [60] involved in hydrogen bondings with different strengths. The broad shoulder below 3000 cm^{-1} for the 2/1 samples corresponds to the OH stretching mode of hydroxyl groups and interlayer water molecules hydrogen bonded to interlayer carbonate anions [61,62].

The presence of water molecules is also responsible for the medium intensity band close to 1635 cm^{-1} (bending mode) in the spectra of the Al-poor samples, which relative intensity decreases because of the development of a stronger band at ca. 1575 cm^{-1} attributed to an overtone of the lattice Al–O mode.

The strongest band in this wavenumber range for the 01 samples within each series is due to mode ν_3 of interlayer carbonate species. As the aluminum content is increased, a shoulder at 1380 cm^{-1} develops, which becomes the strongest band in the 05 samples, and shifts towards higher wavenumbers. This process is accompanied by development of a weak, sharp, band at 1077 cm^{-1}, due to mode ν_1, unactive for a D_{3h} symmetry of the carbonate anion, but active upon a symmetry decrease to C_{3v} or C_{2v}. However, it should be remembered that the PXRD diagrams (Fig. 1) of these Al-rich samples show, in addition to the diffraction maxima of the hydrotalcite-type structure, weak maxima due to the presence of $NaAlCO_3(OH)_2$ are also recorded. Consequently, the presence of carbonate in two different environments in samples with appreciable amounts of Al (and of Na) would account for such an observation.

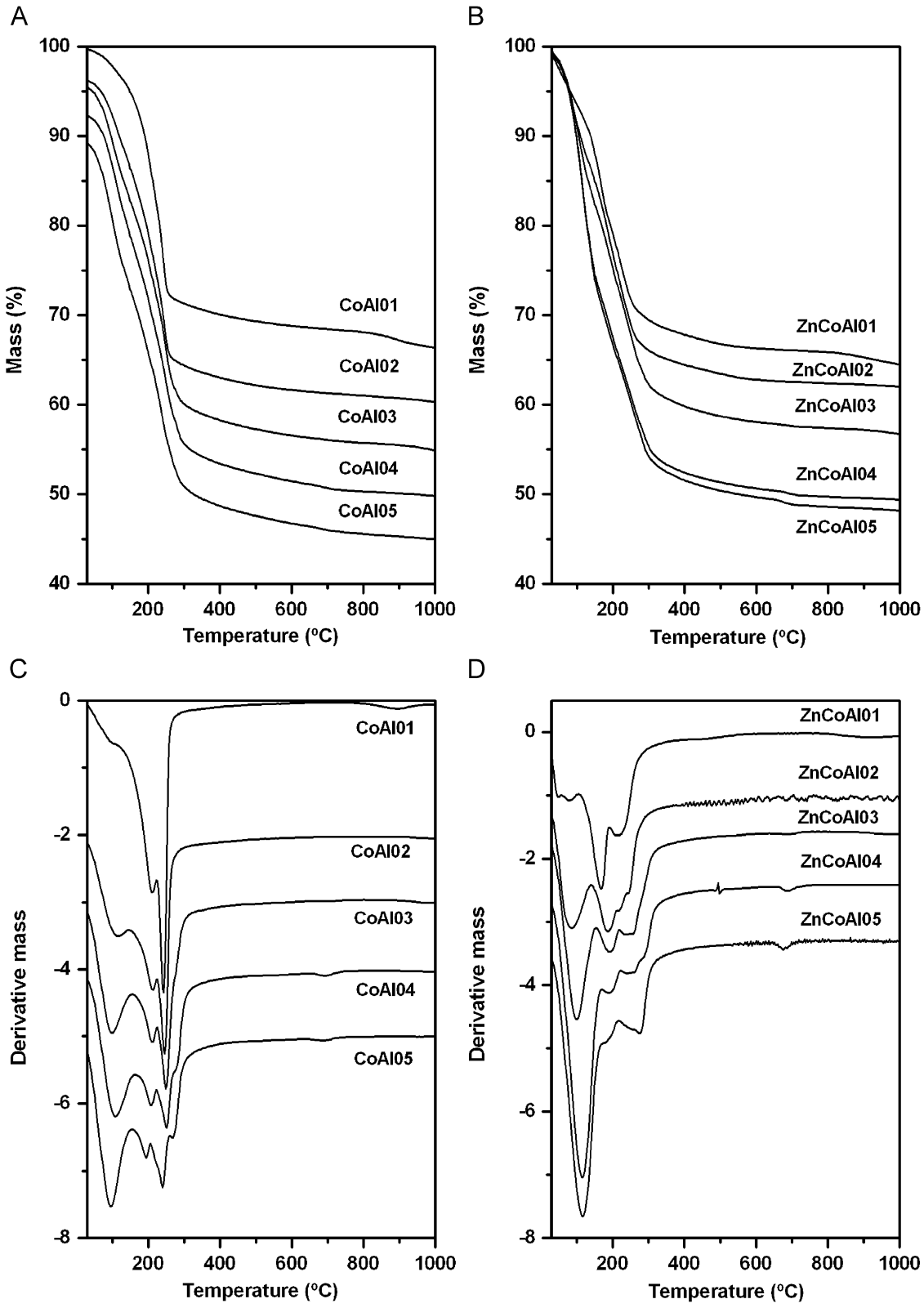

Fig. 3. Thermogravimetric (A and B) and derivative thermogravimetric (C and D) curves for samples CoAl0*X* (A and C) and ZnCoAl0*X* (B and D).

Bands at lower wavenumbers are due to lattice vibration modes and modes ν_2 and ν_4 of carbonate. The presence of different phases, especially in the Al-rich samples (hydrotalcite, gibbsite, boehmite, and dawsonite) where similar polyatomic moieties containing aluminum exist would give rise to bands in close positions in the FT-IR spectra, leading to a difficult precise ascription.

3.5. Temperature-programmed reduction

The profiles recorded for the Zn-free samples are included in Fig. 5A and show a single peak with shoulders, more evident as the amount of aluminum is increased. All curves are referred to a given amount of sample, and the evident decrease in the area under the

curve corresponds to a lower hydrogen consumption as the amount of reducible Co^{II} species is decreased. Under the experimental conditions used, Al^{III} ions are not reduced, and carbonate is decomposed (or released as CO_2) before being reduced to carbon or other species [63]. Reduction starts approximately at the same temperature in all five cases, 380–400 °C, and the position of the maximum shifts towards higher temperatures on passing from sample CoAl01 (ca. 530 °C) to sample CoAl02 (600 °C), and remains at 600±20 °C for the other samples. Previous studies [63] with Co-containing hydrotalcites have shown that under these experimental conditions Co^{II} species are quantitatively reduced to the zero-valent state. Consequently, the (H_2 consumed)/(cobalt content) ratio should be equal to unity. The presence of different components in the reduction profile might be due to (i) the presence of cobalt in different oxidation states, and/or (ii) reduction of structurally different cobalt species. The experimental (H_2 consumed)/(cobalt content) ratios are given in Table 1. This ratio is roughly equal to unity (1.04) for samples CoAl01 and CoAl02, increases up to 1.10 for sample CoAl03 and finally 1.31 for the two remaining samples within this series. Although a deviation up to 10% is generally admitted for this technique, the difference found for samples CoAl04 and CoAl05 is well above the experimental error. As Al^{III} ions are not reduced under these experimental conditions, we conclude that during the thermal treatment and before reduction starts, a portion of the Co^{II} species is oxidized to Co^{III}. The experimental value for the ratio, 1.31, corresponds to an average oxidation state for cobalt of +2.62, i.e., roughly equal to that existing in Co_3O_4 spinel. We can tentatively assume that under the experimental conditions used, Co^{II} species are partially oxidized, and then become reduced to the zero-valent state during the TPR experiment. Probably, the presence of increasing amounts of dawsonite for the Al-rich samples, as confirmed by the PXRD results, favours such an oxidation process.

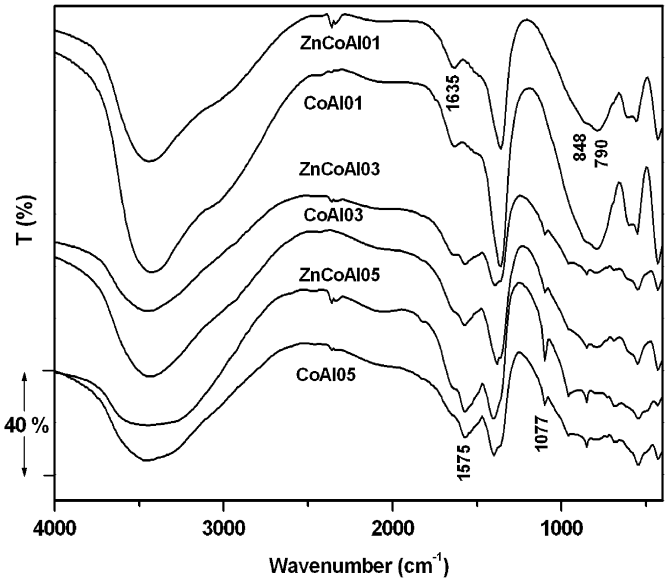

Fig. 4. FTIR spectra of selected samples from both series.

The curves for the Zn-containing samples are included in Fig. 5B. Again a single peak, with at least one shoulder, is recorded in all cases. The position of the main peak is shifted towards higher temperatures than for the Zn-free sample with the same divalent/Al molar ratio, indicating that in this case reduction is more difficult. The maximum is now recorded at ca. 580 °C for

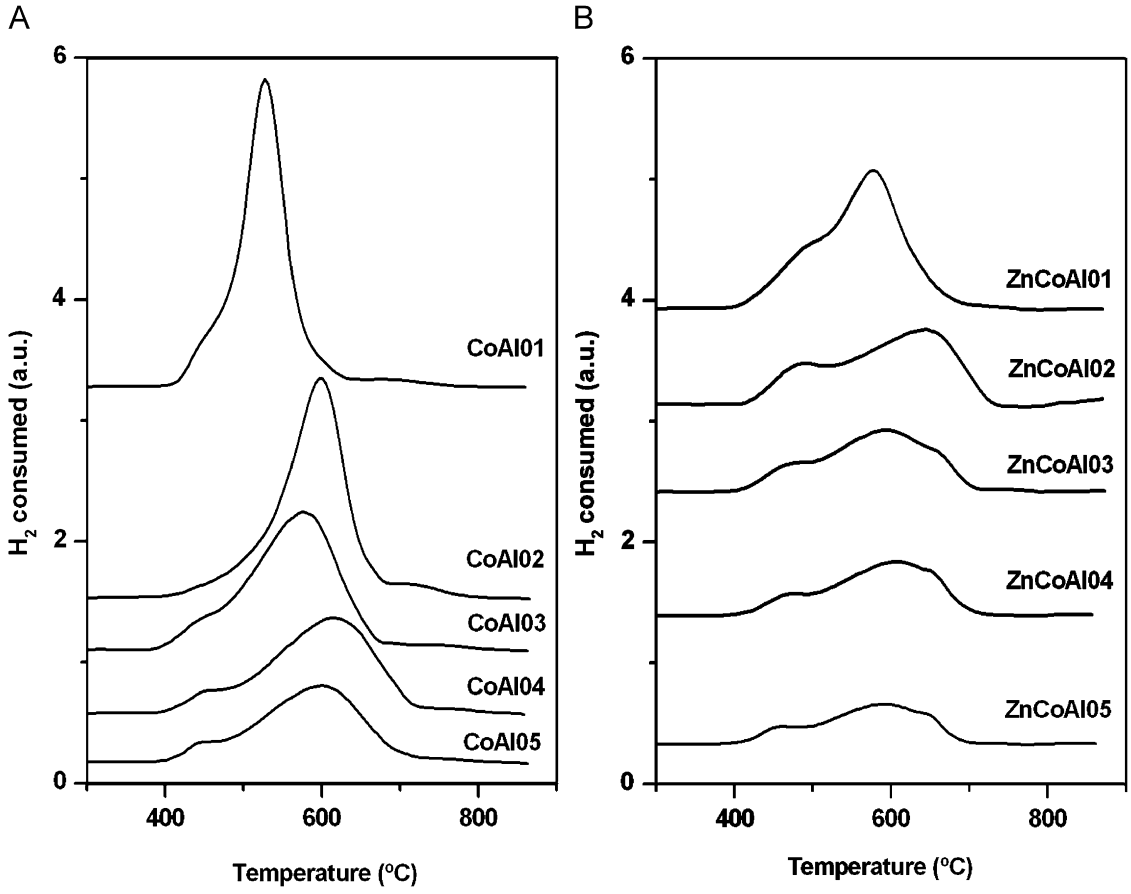

Fig. 5. Temperature-programmed reduction curves for samples (A) CoAl0*X*, and (B) ZnCoAl0*X*.

sample ZnCoAl01, and a shoulder is evident at ca. 470 °C. The (H_2 consumed)/(cobalt content) ratios are 1.46 ± 0.07, i.e., much larger than that corresponding to the transient formation of Co_3O_4, 1.33, and approaching that corresponding to Co_2O_3 (1.50). All these samples contain Zn and the Zn/Co molar ratio is roughly equal to unity. Although crystalline ZnO is not reduced under our experimental conditions, it is feasible that reduction of some Zn^{II} species takes place for ZnCoAl0*X* samples, although this has not been observed in previous studies [43]. ZnO develops lattice defects when heated under vacuum or under reducing conditions, leading to the formation of non-stoichiometric $Zn_{1+x}O$ [64–66]. Lack of reduction of ZnO is probably due to the high stability of well crystallised ZnO; however, in the case of hydrotalcite the lattice should be much more sensitive to the formation of lattice defects, as the layers contain cations with different ionic radii and then the possibility of ion diffusion and lattice defects generation should be noticeably larger than in well crystallised brucite or ZnO [67]. In other words, Zn^{II} species seem to undergo partial reduction along the TPR experiments, together with the cobalt species. Unfortunately, as we cannot quantify the extension of Zn^{II} reduction, an assessment of the average oxidation state of the cobalt species cannot be achieved with the experimental techniques available.

3.6. Particle size distribution

Application of these materials as ceramic pigments is only possible if particles have a given size and the performance is improved if the particle size distribution is narrow. The particle size distribution of our samples, submitted to ultrasounds (US) *in situ*, are shown in Fig. 6. For simplicity, only the curves for the extreme samples within each series are shown.

The distribution depends mostly on the divalent/Al molar ratio, whichever the precise nature of the divalent cations existing in the samples (Co or Co and Zn). This behaviour must be related to formation of a single (Al-poor samples) or mixed phases (Al-rich samples). For samples CoAl01 and ZnCoAl01 the maximum of the curve is found for a particle size of 30 μm, while for samples CoAl05 and ZnCoAl05 the maximum is recorded for a particle size of 65 μm. Moreover, for the former pair of samples the distribution is very narrow, and no particles with a diameter larger than 100 μm are found, while the distribution is noticeably broader for the Al-rich samples; in this case the curve shows some sort of asymmetry and a weak contribution by particles with a diameter around 500 μm can be envisaged.

3.7. Study of the calcined solids

The samples prepared can be applied as such when used as pigments, but they will be then submitted to firing at temperatures around 1000 °C. Alternatively, they can be calcined and then applied, undergoing a second firing treatment in this case. Whichever the route used, it is interesting to know the properties of the calcined solids, as they will appear in the final application. For these reasons, we have submitted the samples to calcination at 1200 °C at a heating rate of 10 °C/min, with a retention time of 5 h. The calcined samples will be named as XXX/1200, where XXX stands for the name given to the uncalcined solid.

The weight loss upon calcination ranged between ca. 35% and 48% of the initial sample weight, increasing within this range as the content in trivalent metal was increased. For a given nominal divalent/trivalent ratio, weight losses for the ZnCo/Al system were larger than for the Co/Al one.

The PXRD diagrams for three selected samples (M^{II}/Al molar ratios 2/1, 1/1, and 1/2) within each series are shown in Fig. 7.

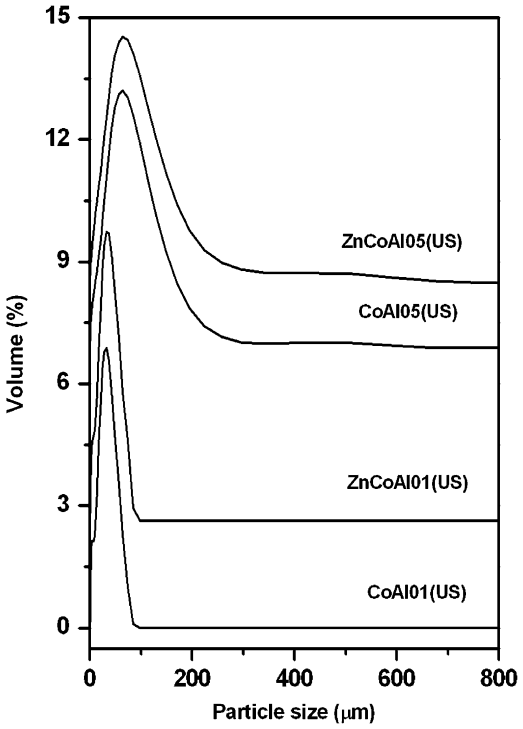

Fig. 6. Particle size distribution curves for selected samples from both series.

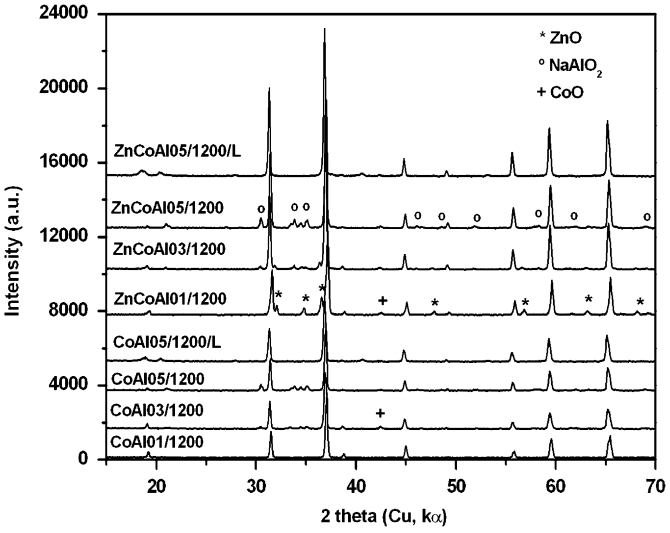

Fig. 7. Powder X-ray diffraction diagrams for selected samples from both series.

All peaks recorded for sample CoAl01/1200 are coincident (position and relative intensity) with those for Co_2AlO_4 (JCPDS file 38-0814), which chemical composition (Co/Al molar ratio) is also coincident with that in the starting solutions used to prepare the sample, and also from the analysis of the residues from the DTA study. These maxima are also recorded in the diagram of sample CoAl05/1200, where some additional weak peaks, due to $NaAlO_2$ (JCPSD file 33-1200), are also recorded (see the 33–37 2θ range) and weaker peaks in the same positions are recorded for sample CoAl03/1200 (Co/Al molar ratio 1/1). This finding is not surprising, as these samples contained detectable amounts of sodium which is not removed during the thermal treatments.

It should be remembered that all spinels potentially formed containing Zn, Co, Al have very similar chemical compositions and lattice parameters, so their diffraction maxima are expected in very close positions. Lattice parameter *a* is 8.1030 Å ($CoAl_2O_4$),

8.0860 Å (Co_2AlO_4), and 8.0840 Å (Co_3O_4) [68]. For our samples the values are 8.056 Å (CoAl01/1200), 8.076 Å (CoAl03/1200) and 8.085 Å (CoAl05/1200); a slight increase in the value of the lattice parameters is observed as the Co content decreases, but this cannot be related to an increase in the Al content as the ionic radius of Al^{III} (0.53 Å in tetrahedral coordination and 0.675 Å in octahedral coordination) [51] is lower than the ionic radii of Co^{II} or Co^{III} species. The trend observed can be tentatively related to an increase in the content of Co^{II} species, as its radius (0.74 Å in tetrahedral coordination and 0.885 Å in high-spin octahedral coordination) is always larger than that for Co^{III} (0.685 Å for low spin octahedral coordination and 0.75 Å for high-spin octahedral coordination). In other words, the Co^{II} (Co^{III}) content in the spinel formed would increase (decrease) as the aluminum content is increased.

The calcined samples containing $NaAlO_2$ were washed by suspending them in water at room temperature for 1 h and magnetic stirring, and then were filtered and dried at room temperature for 3 h. The corresponding PXRD diagrams for some of the washed samples (denoted with the same name, but an "L" appended) are shown also in Fig. 7. As it can be seen, all peaks corresponding to diffraction by $NaAlO_2$ planes have been removed, and the remaining ones correspond solely to a spinel phase. Removal of $NaAlO_2$ has been also checked by FT-IR spectroscopy; and the expected bands of this phase at 920–800 and ca. 450 cm^{-1} are absent. In other words, although the presence of large amounts of aluminum gives rise to retention of sodium in the solids as $NaAlO_2$, this can be easily removed before application of the pigment by a simple washing step at room temperature.

Fig. 7 includes also the PXRD diagrams for the corresponding Zn-containing solids. The peaks are somewhat more intense and sharper than for the corresponding Zn-free samples, suggesting a larger crystallinity. The positions of the main peaks are coincident with those of different spinels, Co_2AlO_4 (JCPDS file 38-0814), $ZnAl_2O_4$ (gahnite, JCPDS file 05-0669) and $ZnCo_2O_4$ (JCPDS file 1-1149), but again the extreme closeness of the ionic radii of the cations (0.75 Å in tetrahedral coordination and 0.88 Å in octahedral coordination for Zn^{II}) makes extremely difficult to ascertain the precise spinel formed; the lattice parameters for spinels $ZnAl_2O_4$ and $ZnCo_2O_4$ are 8.0848 and 8.0946 Å, respectively (8.075, 8.060, and 8.087 Å for samples ZnCoAl01/1200, ZnCoAl03/1200, and ZnCoAl05/1200, respectively). Formation of a mixture of different spinels cannot be ruled out. We have previously found [69] that calcination of Co^{II}–Fe^{III} LDHs at 400 °C leads to formation of a single spinel phase, but the positions of the maxima recorded do not coincide with those for any spinel reported in the JCPDS database; when the calcination temperature is increased, splitting of the maxima is observed and a mixture of two stoichiometric spinels is concluded. In addition, sample ZnCoAl01/1200 also displays some diffraction maxima due to ZnO (JCPDS file 05-0669) which are also recorded, although with a lower intensity, for sample ZnCoAl03/1200, but are absent in the diagrams of the Al-richer samples, suggesting that in these two samples all Zn has been incorporated into a spinel phase. As for the Zn-free samples, an increase in the Al content (and retention of increasing amounts of sodium) gives rise to formation of $NaAlO_2$, which diffraction maxima are recorded for samples with M^{II}/Al molar ratios of 1/1 and above. On washing the $NaAlO_2$ residues are removed.

An extremely weak diffraction line close to 42.5° (2θ) is recorded in the diagram of sample CoAl03/1200 and for all Zn-containing samples, although its intensity decreases as the Co content does. This diffraction line might correspond to CoO (JCPDS file 09-0402). Its formation in sample CoAl01/1200 can be explained from results for element chemical analysis, as the Co/Al molar ratio for this sample was somewhat larger than the stoichiometric one for the Co_2AlO_4 spinel (see Table 1). However, the diffraction line for this phase persists for the Zn-containing samples even when the Co content decreases, while the lines for ZnO vanish for large Al contents. It seems that spinels containing Zn are preferentially formed than spinels containing Co in this series of samples.

The TPR curves for selected calcined samples are shown in Fig. 8. Each series of samples show a different behaviour, highlighting the role played by Zn on the reducibility of these solids. So, regarding samples CoAl0*X*/1200, up to three different reduction steps are recorded, the first one around 400 °C, which relative intensity progressively decreases as the Al content increases. The amount of hydrogen consumed for each sample always exceeds the amount calculated if all cobalt species are in the divalent oxidation state. As the PXRD data suggest the presence of spinels containing Co^{III} cations, we should conclude that a partial oxidation of Co^{II} to Co^{III} has taken place during calcination. From the Co content and the amount of hydrogen consumed, and bearing in mind that during the reduction processes 1 and 1.5 mol of hydrogen are consumed, respectively, to reduce 1 mol of Co^{II} and 1 mol of Co^{III}, the content of these two species of cobalt can be calculated; results are summarised in Table 4. The amount of Co^{II} roughly increases as the aluminum content is increased, in agreement with the presence of increasing amounts of $CoAl_2O_4$ at expenses of a lower content of Co_2AlO_4. The change in the calculated relative content of Co^{II} and Co^{III} in this series of samples does not run parallel to the relative areas of the reduction steps concluded from the TPR curves. Nevertheless, as the area of the first peak decreases as the Co^{III} content does, this low-temperature reduction process should be mostly related to reduction of Co^{III} species. These results are in agreement with the PXRD ones above described, showing a decrease in spinels containing Co^{III} species in the calcined samples as the Al content was increased.

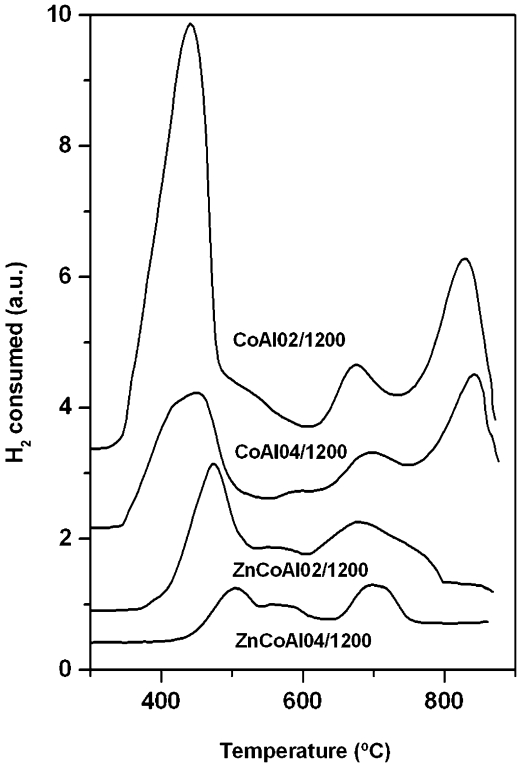

Fig. 8. Temperature-programmed reduction curves for selected samples from both series.

Regarding the Zn-containing samples the situation is somewhat different, as in this case the amount of hydrogen consumed roughly corresponds to the exclusive presence of Co^{III} for samples ZnCoAl0*X*/1200 (*X* = 1, 2, and 3), but of Co^{II} for samples with *X* = 4 and 5 (see Table 4). Up to four different cobalt species have been previously reported by Velu et al. [43] for ZnCoAl LDHs calcined at 300–900 °C, the reduction maxima shifting to higher temperatures as the calcination temperature does; as the presence of Al^{III} ions impedes reduction of cobalt species, these authors [43] conclude that the first reduction maxima are due to reduction of Co_3O_4 or $ZnCo_2O_4$ species (Co species without Al^{III} neighbours), while species like $CoAl_2O_4$ or Al-containing $Co_3O_4/ZnCo_2O_4$ solid solutions are reduced at higher temperatures [43]. Nevertheless, the reduction temperatures in our case are larger than in these studies, indicating a larger stability of the phases formed. Although we could assume also for this series of samples a partial reduction of Zn^{II} species, such a reduction probably does not take place due to the high crystallinity of these calcined samples.

The results obtained suggest that in this ZnCoAl0*X*/1200 series of samples, Co cations are mostly in the divalent state for low cobalt content (*X* = 1, 2, and 3), probably forming a Co_2AlO_4 spinel, while for samples with *X* = 4 and 5 the spinel formed should be closer to $CoAl_2O_4$. However, due to the closeness among the ionic radii of the cations existing in these compounds, formation of a continuous series of spinels, which precise composition critically depends on the chemical composition of the starting LDH, cannot be ruled out.

3.8. Colour properties

Colour properties of all 10 precursors and 10 calcined products have been measured and the *L**, *a** and *b** parameters have been determined. Values for *L** are plotted in Fig. 9A and those for coordinates *a** and *b** in Fig. 9B.

As it can be seen in Fig. 9A, the luminosity of the samples depends mostly on: (i) if they have been submitted or not to any calcination treatment, and (ii) the existing cations. It should be noted that with a given series of samples the molar fractions of the containing cations has a weaker effect. So, all CoAl0*X* samples show luminosity values ranging from 35 to 40. Such a range is somewhat narrower for the ZnCoAl0*X* samples (ca. 41–44), but in both cases the values are rather high.

On the contrary, the values form samples CoAl0*X*/1200 are much lower and spanning in an even narrower range (4–7) and so they can be considered independent on its precise chemical composition. Regarding samples ZnCoAl0*X*/1200 the luminosity is lower than for the uncalcined samples, but extending in a broader range (6–17). Roughly speaking, it is observed in all series that luminosity decreases as the cobalt content increases. This finding is somewhat surprising, as the other cations in the samples (Zn^{II} and Al^{III}) are colourless and then one would expect that an increase in the concentration of the coloured cation would give rise to a lower luminosity. However, we should also consider that the colour of octahedrally coordinated Co^{II} species (pink) is not very intense (as it corresponds to simultaneous excitation of two electrons) and that, according to the TPR results, Co could exist in both the divalent and trivalent state in these samples and then darkening would arise from the presence of octahedrally coordinated Co^{III} species.

The larger luminosity of the ZnCoAl0*X* samples should be related to the important presence of colourless Zn^{II} cations in these samples, where the molar Co/Zn ratio is equal to unity.

Regarding the calcined samples, their markedly lower luminosity should be undoubtedly related to formation of the spinels and migration of Co^{II} species to tetrahedral sites in the spinel structure. The ZnCoAl0*X*/1200 set of samples maintains a slightly larger luminosity than the Zn-free ones, the same behaviour as for the uncalcined corresponding series.

Concerning the changes observed in chromatic coordinates *a** and *b**, grouping mostly depends on a given series, whichever the precise molar ratio between the component cations. So, the uncalcined samples show rather large *a** values, which correspond to a reddish colour. The values for the Zn-containing samples are all them very close to each other, while for the Zn-free samples an increase in parameter *b** (with only a small variation in parameter *a**) is observed as the cobalt content is decreased.

On the contrary, once the samples have been calcined, the opposite behaviour is observed, i.e., closer values of (*a**, *b**) pairs are measured for samples CoAl0*X*/1200 (dark blue) than for samples ZnCoAl0*X*/1200 (dark green).

Table 4
Summary of TPR results for the calcined solids.

Sample	H_2 consumption (exptl./theor.)	Co^{II}[a]	Co^{III}[a]
CoAl01/1200	1.38	24	76
CoAl02/1200	1.28	43	57
CoAl03/1200	1.34	32	68
CoAl04/1200	1.27	46	54
CoAl05/1200	1.23	54	46
ZnCoAl01/1200	1.52	0	100
ZnCoAl02/1200	1.50	0	100
ZnCoAl03/1200	1.47	5	95
ZnCoAl04/1200	1.02	95	5
ZnCoAl05/1200	1.08	83	17

[a] Molar fraction.

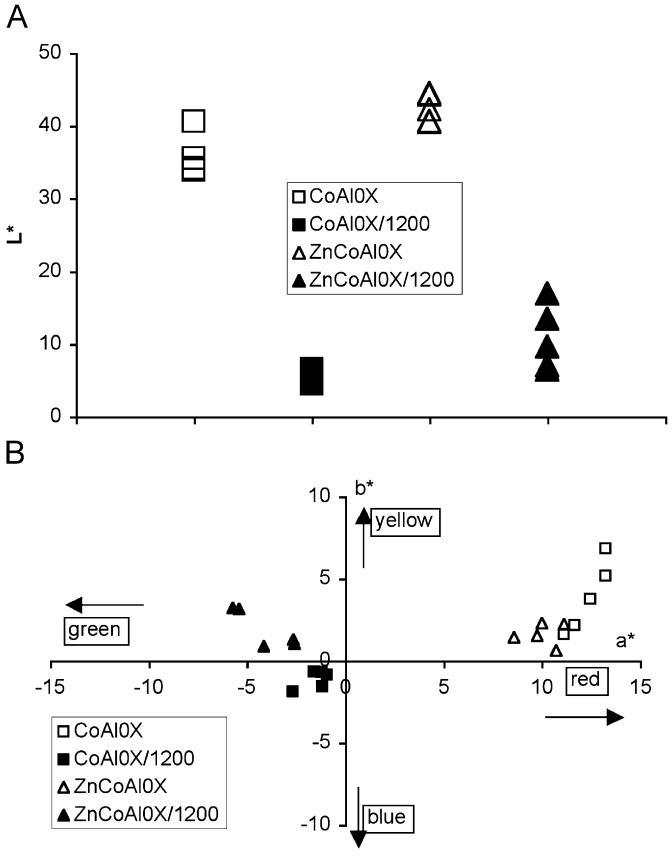

Fig. 9. Luminosity (A) and chromatic coordinates (B) for both series of original and calcined samples.

In this case the Zn-free samples show negative values for a^* (greenish) and b^* (blue), while samples ZnCoAl0*X*/1200 show positive b^* values.

We have compared the colour parameters of these samples with those for a set of similar solids (i.e., with the same chemical composition) prepared by calcination of mixed chlorides and with the same crystalline structure (mixed spinels). This last set of samples shows a larger luminosity whichever the chemical composition, on comparing with the samples here studied, and luminosity is very dependent on the chemical composition, L^* and a^* increasing with the aluminum content, while parameter b^* is more negative for the Al-rich samples. No effect of the presence of Zn is observed. The sample reported by Pacurariu et al. [9] with the same composition as our ZnCoAl01 sample, but calcined at 900 °C, shows also a larger L^* value, and a^* and b^* values close to 5 and −14, respectively, i.e., the sample is less greenish, but deeper blue. In other words, the samples prepared in this study show a lower luminosity than those reported in previous studies, thus permitting the same level of colour with a lower amount of sample.

From these results, we should conclude that the colour of ceramic pigments containing Co and Al is mostly depending on the presence of additional Zn^{II} cations, and not on the precise molar percentage of the colour-responsible cation (cobalt). The presence of $NaAlO_2$ has no effect on the colour of the calcined solids and is easily removed by gentle washing.

4. Conclusions

Two series of solids with the spinel containing Co and Al, or Co, Zn, and Al, aimed to be used as ceramic pigments, have been prepared by calcination of layered double hydroxides, with different divalent/trivalent molar ratios and Zn/Co molar ratio 1. The crystallinity of the precursors decreases as the aluminum content increases, and formation of other phases, containing sodium is observed in these Al-rich samples. Decomposition of the layered materials at 1200 °C leads to formation of spinels with only minor amounts of other phases (mainly ZnO and CoO), as well as $NaAlO_2$, which is easily removed by washing with water. The particle size of the precursors is also dependent on the divalent/trivalent ratio. While the precursors show a pink colour (lighter for those samples containing Zn), the calcined samples are dark blue or dark green, depending on the absence or presence of zinc. The properties of the calcined solids can be easily tuned from the composition and decomposition procedure of the precursors, providing homogeneous solids.

Acknowledgments

Financial support from MEC (Grant MAT2006-10800-C02-01), ERDF and Junta de Castilla y León (Grant SA024A06) is greatly acknowledged. Authors also thank Dr. M. Herrero and Mr. A. Montero for their assistance to obtain some of the experimental results.

References

[1] M. Llusar, A. Forés, J.A. Badenes, J. Calbo, M.A. Tena, G. Monrós, J. Eur. Ceram. Soc. 21 (2001) 1121.
[2] A.L. Fernández, L. de Pablo, Pigm. Resin Technol. 31 (2002) 350.
[3] Z. Chen, E. Shi, W. Li, Y. Zheng, W. Zhong, Mater. Lett. 55 (2002) 281.
[4] F. Meyer, R. Hempelmann, S. Mathur, M. Veith, J. Mater. Chem. 9 (1999) 1755.
[5] M. Zayat, D. Levy, Chem. Mater. 12 (2000) 2763.
[6] U. Lavrencic Stangar, B. Orel, M. Krajnc, J. Sol–Gel Sci. Technol. 26 (2003) 771.
[7] C. Otero Areán, M. Peñarroya Mentruit, E. Escalona Platero, F.X. Llabrés i Xamena, J.B. Parra, Mater. Lett. 39 (1999) 22.
[8] D.M.A. Melo, J.D. Cunha, J.D.G. Fernandes, M.I. Bernardi, M.A.F. Melo, A.E. Martinelli, Mater. Res. Bull. 38 (2003) 1559.
[9] C. Pacurariu, I. Lazau, D. Becherescu, I. Bobos, Rev. Roum. Chim. 42 (1997) 447.
[10] W. Li, J. Li, J. Guo, J. Eur. Ceram. Soc. 23 (2003) 2289.
[11] A.E. Giannakas, A.K. Ladavos, G.S. Armatas, P.J. Pomonis, Appl. Surf. Sci. 253 (2007) 6969.
[12] L.K.C. de Souza, J.R. Zamian, G.N. da Rocha Filho, L.E.B. Soledade, I.M.G. dos Santos, A.G. Souza, T. Scheller, R.S. Angélica, C.E.F. da Costa, Dyes Pigm. 81 (2009) 187.
[13] F. Cavani, F. Trifirò, A. Vaccari, Catal. Today 11 (1991) 173.
[14] V. Rives (Ed.), Layered Double Hydroxides: Present and Future, Nova Science Pub. Co. Inc., New York, 2001.
[15] F. Wypych, K.G. Satyanarayana (Eds.), Clay Surfaces: Fundamentals and Applications, Elsevier, Amsterdam, 2004.
[16] X. Duan, D.G. Evans (Eds.), Layered Double Hydroxides. Structure and Bonding, vol. 119, Springer, Berlin, 2006.
[17] C. Forano, T. Hibino, F. Leroux, C. Taviot-Guého, in: F. Bergaya, B.K.G. Theng, G. Lagaly (Eds.), Handbook of Clay Science, Elsevier, Amsterdam, 2006 (Chapter 13.1).
[18] F. Kovanda, K. Jiratova, R. Kalouskova, in: F.L. Gerard (Ed.), Advances in Chemistry Research, vol. 1, Nova Science Pub. Co. Inc., New York, 2006, pp. 89–139.
[19] V. Rives, M.A. Ulibarri, Coord. Chem. Rev. 181 (1999) 61.
[20] M. del Arco, E. Cebadera, S. Gutiérrez, C. Martín, M.J. Montero, V. Rives, J. Rocha, M.A. Sevilla, J. Pharm. Sci. 93 (2004) 1649.
[21] D. Carriazo, M. del Arco, C. Martín, V. Rives, Appl. Clay Sci. 37 (2007) 231.
[22] M. del Arco, D. Carriazo, C. Martín, A.M. Pérez-Grueso, V. Rives, Mater. Sci. Forum 514–516 (2006) 1541.
[23] V. Rives, O. Prieto, A. Dubey, S. Kannan, J. Catal. 220 (2003) 161.
[24] A. Dubey, V. Rives, S. Kannan, J. Mol. Catal. A: Gen. 181 (2002) 151.
[25] V. Rives, A. Dubey, S. Kannan, Phys. Chem. Chem. Phys. 3 (2001) 4826.
[26] F. Iosif, V.I. Parvulescu, M.E. Pérez-Bernal, R.J. Ruano-Casero, V. Rives, K. Kranjc, S. Polanc, M. Kocevar, E. Genin, J.P. Genet, V. Michelet, J. Mol. Catal. A: Gen. 276 (2007) 34.
[27] A. Monzón, E. Romeo, C. Royo, R. Trujillano, F.M. Labajos, V. Rives, Appl. Catal. A: Gen. 185 (1999) 53.
[28] V. Rives, F.M. Labajos, R. Trujillano, E. Romeo, C. Royo, A. Monzón, Appl. Clay Sci. 12 (1998) 363.
[29] P. Benito, M. Herrero, F.M. Labajos, V. Rives, C. Royo, N. Latorre, A. Monzón, Chem. Eng. J. 149 (2009) 455.
[30] S. Blanco, S.R.G. Carrazán, V. Rives., Appl. Catal. A: Gen. 342 (2008) 93.
[31] M.E. Pérez-Bernal, R.J. Ruano-Casero, V. Rives, Ceram.-Silik. 48 (2004) 145.
[32] A. Sánchez, M.E. Pérez-Bernal, R.J. Ruano-Casero, V. Rives, in: M. Suárez, M.A. Vicente, V. Rives, M.J. Sánchez (Eds.), Materiales Arcillosos: de la Geología a las Nuevas Aplicaciones, Varona, Salamanca, 2006, pp. 151–164.
[33] R.J. Ruano-Casero, M.E. Pérez-Bernal, V. Rives, Z. Anorg. Allg. Chem. 631 (2005) 2142.
[34] J.M. García-García, M.E. Pérez-Bernal, R.J. Ruano-Casero, V. Rives, Solid State Sci. 9 (2007) 1115.
[35] M.E. Pérez-Bernal, R.J. Ruano-Casero, F. Benito, V. Rives, J. Solid State Chem. 182 (2009) 1593.
[36] C. Barriga, J.M. Fernández, M.A. Ulibarri, F.M. Labajos, V. Rives, J. Solid State Chem. 124 (1996) 205.
[37] V. Rives, F.M. Labajos, M.A. Ulibarri, P. Malet, Inorg. Chem. 32 (1993) 5000.
[38] F.M. Labajos, V. Rives, P. Malet, M.A. Centeno, M.A. Ulibarri, Inorg. Chem. 35 (1996) 1154.
[39] I. Crespo, C. Barriga, M.A. Ulibarri, G. González-Bandera, P. Malet, V. Rives, Chem. Mater. 15 (2001) 1518.
[40] J.M. Fernández, M.A. Ulibarri, F.M. Labajos, V. Rives, J. Mater. Chem. 8 (1998) 2507.
[41] M. Herrero, P. Benito, F.M. Labajos, V. Rives, Catal. Today 128 (2007) 129.
[42] M. Herrero, P. Benito, F.M. Labajos, V. Rives, J. Solid State Chem. 180 (2007) 873.
[43] S. Velu, K. Suzuki, S. Hashimoto, N. Satoh, F. Ohashi, S. Tomura, J. Mater. Chem. 11 (2001) 2049.
[44] R.K. Mason, Am. Ceram. Soc. Bull. 40 (1961) 5.
[45] P. Escribano, J.B. Carda, E. Cordoncillo, Esmaltes y Pigmentos Cerámicos, Enciclopedia Cerámica, vol. 1, Faenza Editrice Ibérica SL, Castellón, 2001.
[46] S. Kannan, A. Narayanan, C.S. Swamy, J. Mater. Sci. 31 (1996) 2353.
[47] P. Gay, The Crystalline State, an Introduction, Oliver & Boyd, Edinburgh, 1972.
[48] A.S. Bookin, V.I. Cherkashin, V.A. Drits, Clays Clay Miner 41 (1993) 631.
[49] M.A. Ulibarri, F.M. Labajos, V. Rives, R. Trujillano, W. Kagunya, W. Jones, Inorg. Chem. 33 (1994) 2592.
[50] V.A. Drits, A.S. Bookin, in: V. Rives (Ed.), Layered Double Hydroxides: Present and Future, Nova Sci. Pub. Co. Inc., New York, 2001 (Chapter 2).
[51] R.D. Shannon, C.T. Prewitt, Acta Crystallogr. B 25 (1969) 925.
[52] R. Jenkins, J.L. de Vries, Worked Examples in X-ray Analysis, second ed., Philips Technical Library, MacMillan Press Ltd., London, 1978.
[53] H.P. Klug, L.E. Alexander, X-ray Diffraction Procedures, Wiley, New York, 1974.
[54] J. Pérez-Ramírez, G. Mul, J.A. Moulijn, Vibr. Spec. 27 (2001) 75.
[55] L. Chmielarz, P. Kustrowski, A. Rafalska-Lasocha, A. Majda, R. Dziembaj, Appl. Catal. B: Environ. 35 (2002) 195.
[56] M.A. Ulibarri, J.M. Fernández, F.M. Labajos, V. Rives, Chem. Mater. 3 (1991) 626.
[57] I. Guinea, I. M.Sc. Thesis, University of Salamanca, 2005.
[58] V. Rives, Inorg. Chem. 38 (1999) 406.
[59] P. Bera, M. Rajamathi, M.S. Hedge, P.V. Kamath, Bull. Mater. Sci. (India) 23 (2000) 141.

[60] K. Nakamoto, Infrared and Raman Spectra of Inorganic and Coordination Compounds, fifth ed, Wiley, New York, 1997.
[61] J.T. Kloprogge, R.L. Frost, in: V. Rives (Ed.), Layered Double Hydroxides: Present and Future, Nova Sci. Pub. Co. Inc., New York, 2001 (Chapter 5).
[62] J.T. Kloprogge, in: J.T. Kloprogge (Ed.), The Application of Vibrational Spectroscopy to Clay Minerals and Layered Double Hydroxides, CMS Workshop Lectures, vol. 13, The Clay Minerals Society, Aurora, CO, 2005.
[63] V. Rives, M.A. Ulibarri, A. Montero, Appl. Clay Sci. 10 (1995) 83.
[64] R.J.D. Tilley, Defect Crystal Chemistry and Its Applications, Blackie & Son, Ltd., London, 1987.
[65] N.N. Greenwood, Ionic Crystals, Lattice Defects and Nonstoichiometry, Butterworth, London, 1968.
[66] N.N. Greenwood, A. Earnshaw, Chemistry of the Elements, second ed, Butterworth, Oxford, 1998.
[67] C. Barriga, f. Kooli, V. Rives, M.A. Ulibarri, in: M.L. Occelli, H. Kessler (Eds.), Synthesis of Porous Materials: Zeolites, Clays and Nanostructures, Marcel Dekker, Inc., New York, 1997, pp. 661–674 (Chapter41).
[68] JCPDS: Joint Committee on Powder Diffraction Standards, International Centre for Diffraction Data, Pennsylvania, 1977.
[69] M. del Arco, R. Trujillano, V. Rives, J. Mater. Chem. 8 (1998) 761.